Bioconjugate Chemistry

pubs.acs.org/bc

Article

Lectin-Functionalized Chitosan Nanoparticle-Based Biosensor for Point-of-Care Detection of Bacterial Infections

Kapil Punjabi,* Rishi Rajat Adhikary, Aishani Patnaik, Prachi Bendale, Survanshu Saxena, and Rinti Banerjee

Cite This: *Bioconjugate Chem.* 2022, 33, 1552–1563

Read Online

ACCESS | Metrics & More | Article Recommendations | Supporting Information

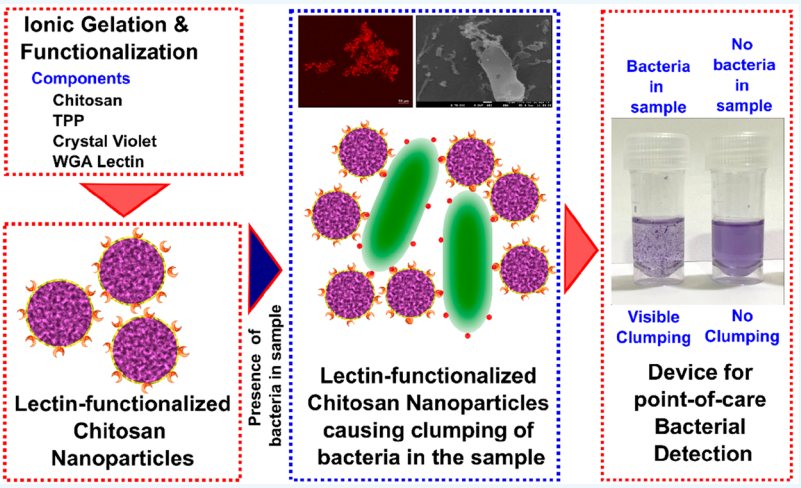

ABSTRACT: The WHO estimates an average of 10 million deaths per year due to the increasing number of infections and the predominance of drug resistance. To improve clinical outcomes and contain the spread of infections, the development of newer diagnostic tools is imperative to reduce the time and cost involved to reach the farthest population. The current study focuses on the development of a point-of-care technology that uses crystal violet entrapped, lectin functionalized chitosan nanoparticles to detect the presence of clinically relevant bacterial infections. Spherical nanoparticles of <200 nm in diameter make up the biosensing nanomaterial, showed specific clumping in the presence of bacteria to form visible aggregates as compared to a nonbacterial sample. Visible agglutination confirmed the presence of bacteria in the samples. The devices require just 100 μL of sample and were tested with various bacteria-spiked saline, simulated urine, artificial sputum, and simulated respiratory and wound swabs. The developed device did not require any sample preparation or sophisticated instruments while enabling rapid differentiation between bacterial and nonbacterial infections within 10 min. The *in vitro* results with bacteria-spiked simulated samples reveal 100% sensitivity and specificity with a limit of detection of 10^5 cfu/mL. The nanomaterial developed was found to be stable for more than 90 days at accelerated conditions. The developed device can be a screening tool for home-based or clinical assessment and follow the treatment accordingly, reducing exposure to broad-spectrum antibiotics in the case of nonbacterial infections.

INTRODUCTION

According to the World Health Organization (WHO) in 2016, bacterial infections were ranked in the top causes of deaths worldwide, accounting for more than 6 million annually.[1] Often infections are treated symptomatically using broad-spectrum antibiotics without determining the causal organism due to limited access to basic and rapid diagnosis.[2] This leads to irrational use of antibiotics and development of antibiotic resistance, which can further lead to deteriorating clinical outcomes and increased morbidity and mortality. Thus, there is a need to distinguish bacterial infections from nonbacterial infections.

Diagnostic technologies have substantially improved over the years especially in the developed countries. Laboratory-based testing has become gradually automated, which has improved consistency and reduced operator time.[3] These improved technologies require skilled personnel and sophisti-

Received: June 27, 2022
Revised: July 17, 2022
Published: August 3, 2022

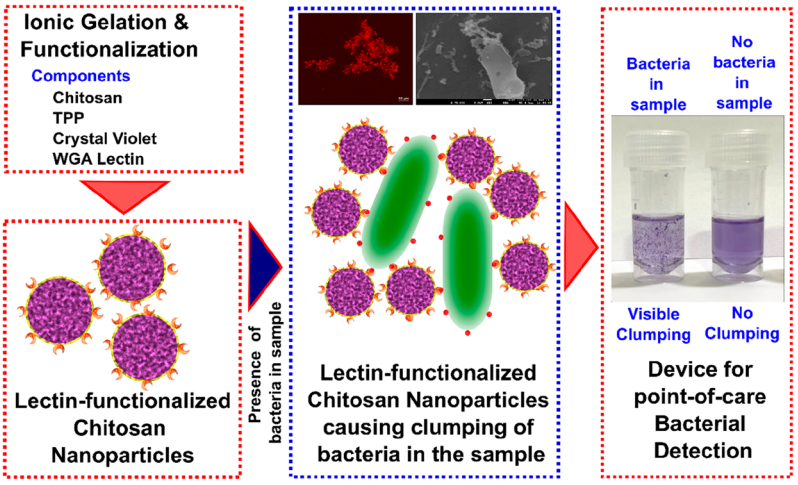

Figure 1. Graphical scheme of the developed biosensor.

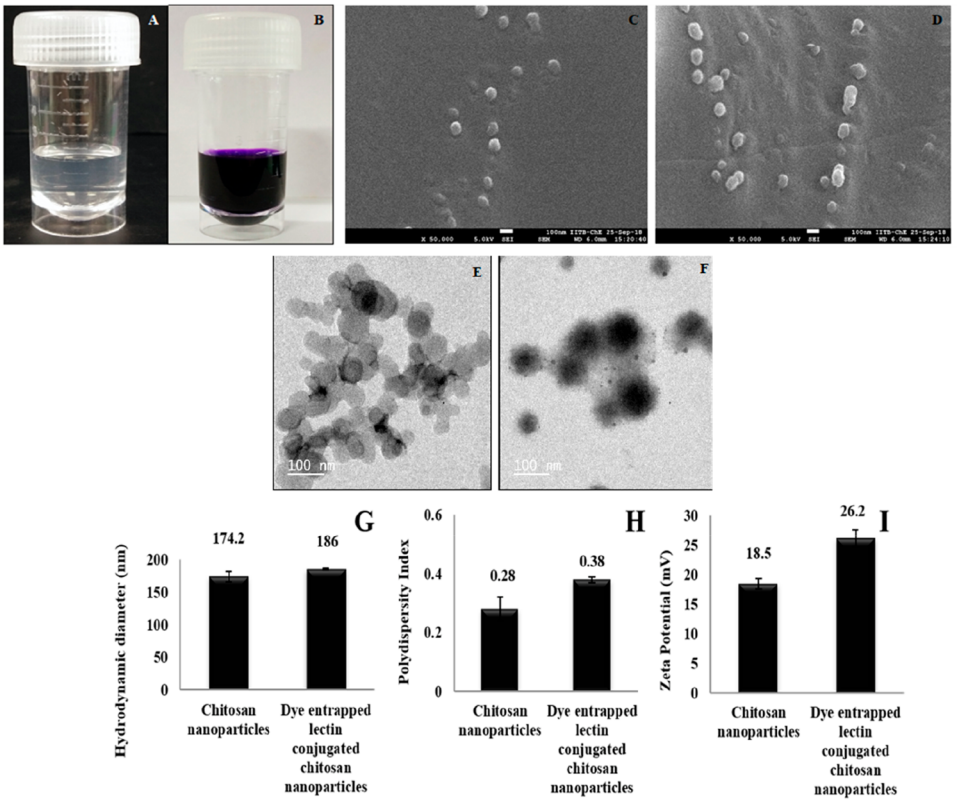

Figure 2. Characterization of nanoparticles. (A) Chitosan nanoparticles; (B) Dye entrapped lectin conjugated chitosan nanoparticles. SEM: (C) Dye entrapped chitosan nanoparticles; (D) Dye entrapped lectin conjugated chitosan nanoparticles. TEM: (E) Dye entrapped chitosan nanoparticles; (F) Dye entrapped lectin conjugated chitosan nanoparticles. (G) Hydrodynamic diameter. (H) Polydispersity Index (PDI). (I) Zeta Potential.

cated instruments. Patients in developing countries are treated at healthcare facilities that do not have requisite diagnostic facilities. One of the greatest challenges faced today is to develop technologies for a low resource setting. The World Development Report of 2004 mentions lack of accessibility as one of the major reasons for failure of health services.[4] Reduced time of detection (TOD) can prove to be crucial in containing the spread of infections. Studies suggest that a delay in appropriate therapy can lead to longer duration of antibiotic therapy, longer hospital stay, and higher healthcare costs. In certain diseases, such as meningitis, reduced TOD can improve clinical outcome significantly.[5]

Conventionally, bacterial infections are detected by methods such as microscopy, biochemical testing, and culture-based testing.[6] These methods remain the gold standards for bacterial detection. However, the TOD of 24−72 h results in delayed therapy. New age testing heralded the use of molecular recognition moieties and molecular diagnostics like NAAT (nucleic acid amplification testing) using PCRs (polymerase chain reactions), WGS (whole genome sequencing), and

https://doi.org/10.1021/acs.bioconjchem.2c00299
Bioconjugate Chem. 2022, 33, 1552−1563

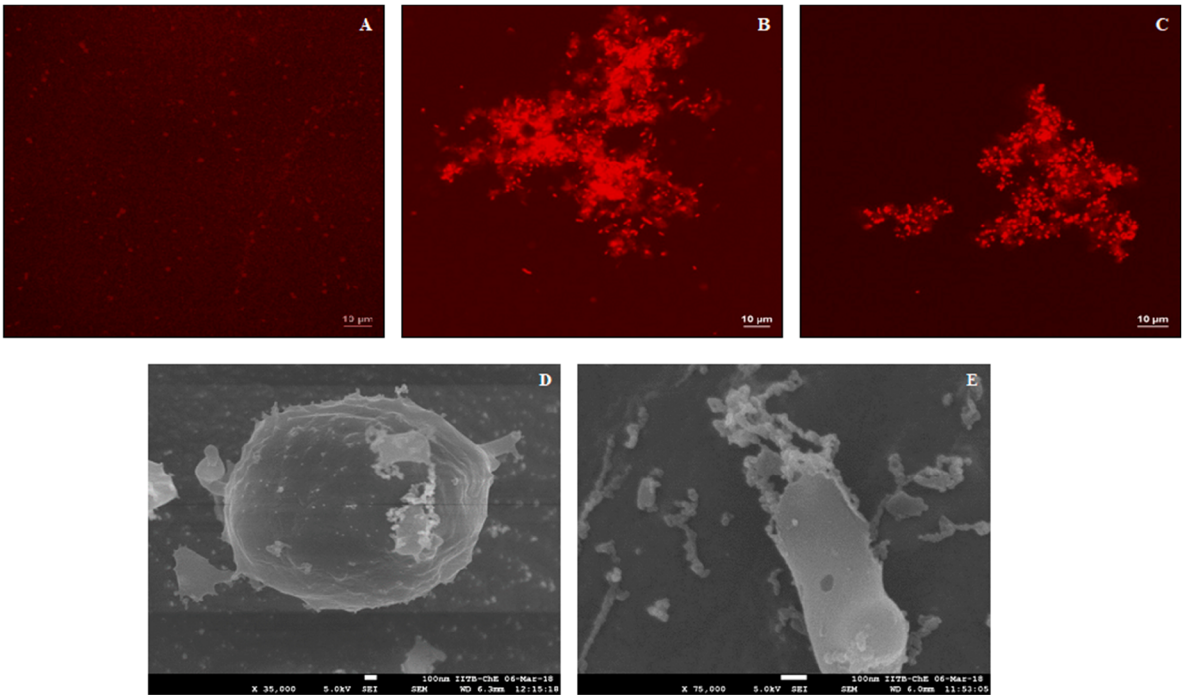

Figure 3. Microscopic confirmation. CLSM: (Top) (A) Dye entrapped lectin conjugated chitosan nanoparticles; (B) agglutination of nanoparticles with Gram-positive *S. aureus*; (C) agglutination and interaction of nanoparticles with Gram-negative *E. coli*; (Bottom) CRYO-FEG-SEM micrographs confirming agglutination of nanoparticles with (D) Gram-positive *S. aureus* and (E) Gram-negative *E. coli*.

microarrays with reduced TOD.[7] However, these require sophisticated instruments, extensive sample processing, expertise, and advanced laboratory setups.[8] To mitigate the disadvantages of a conventional diagnostic method there is a need to develop miniaturized point-of-care devices (POCDs) that follow the "ASSURED" (affordable, sensitive, specific, user-friendly, rapid and robust, equipment-free, and deliverable to end users) guidelines of the WHO.[9] This will lead to a reduced TOD and thus enable clinicians to prescribe appropriate therapy upon differentiating between bacterial and nonbacterial infections.

The phenomenon of miniaturization has led to rapid development in the fields of nanotechnology and bioengineering. Multiple functionalities in these miniaturized systems can be achieved by the use of "smart materials". These smart materials are widely used for diagnostic purposes.[10] Chitosan is a positively charged smart biopolymer produced by deacetylation of chitin. The low cost, biodegradability, and biocompatibility make it a favored polymer for use in biomedical applications.[11] Chitosan nanoparticles can be produced by ionic gelation which is highly tunable, and since cross-linking is through electrostatic attraction, functional groups remain available for biomolecular conjugation with antibodies, proteins, or lectins.[12] Lectins are a class of proteins found in plants and animals, known to be specific to carbohydrates. The lectin−carbohydrate specificity is similar to other commonly known biomolecular recognition interactions such as antibody−antigen and enzyme−substrate. Lectin from *Triticum vulgaris* is known to be specific to N-acetyl glucosamine (NAG), one of the two components that make up the peptidoglycan layer of the bacterial cell wall.[13]

In this paper, we describe a point-of-care diagnostic technology that uses dye entrapped lectin conjugated chitosan nanoparticles for rapid detection of bacteria directly from various samples like urine, sputum, respiratory swabs, and wound swabs by visual agglutination reaction as per Figure 1.

RESULTS

Characterization of Dye Entrapped Lectin Conjugated Chitosan Nanoparticles. Chitosan nanoparticles in a stable suspension appeared to be translucent with no precipitation as seen in Figure 2A. To facilitate visualization of an expected positive result (agglutination), crystal violet was entrapped within the chitosan nanoparticles as shown in Figure 2B). Crystal violet (CV) is a positively charged dye and is known to adhere with the cell walls of both Gram-positive and Gram-negative bacteria; the entrapment of CV in chitosan-TPP nanoparticles is achieved by the strong electrostatic interaction with anionic groups of TPP.

CRYO-FEG-SEM analysis showed spherical chitosan nanoparticles tagged with lectin as shown in Figure 2D. FEG-TEM images of chitosan nanoparticles conjugated with lectin showed a diffuse coating around the particles as seen in Figure 2F. Comparable images of dye entrapped nonconjugated chitosan particles are provided in Figures 2C,E.

The hydrodynamic diameter and polydispersity index (PDI) of conjugated and nonconjugated nanoparticles were determined by dynamic light scattering (DLS) analysis as per Figure 2G,H. The size of the conjugated nanoparticles was 186 ± 1.4 nm as compared to nonconjugated particles, which was 174.2 ± 8.1 nm. Similarly, the zeta potential analysis confirmed a difference in surface charge for conjugated and nonconjugated particles. The surface charge for conjugated nanoparticles was 26.2 ± 1.4 mV, whereas the surface charge for nonconjugated particles was 18.5 ± 0.9 mV as seen in Figure 2I.

Microscopic Confirmation of Agglutination. The microscopic evaluation confirms the agglutination of Gram-positive (*S. aureus*) as well as Gram-negative (*E. coli*) bacteria

https://doi.org/10.1021/acs.bioconjchem.2c00299
Bioconjugate Chem. 2022, 33, 1552−1563

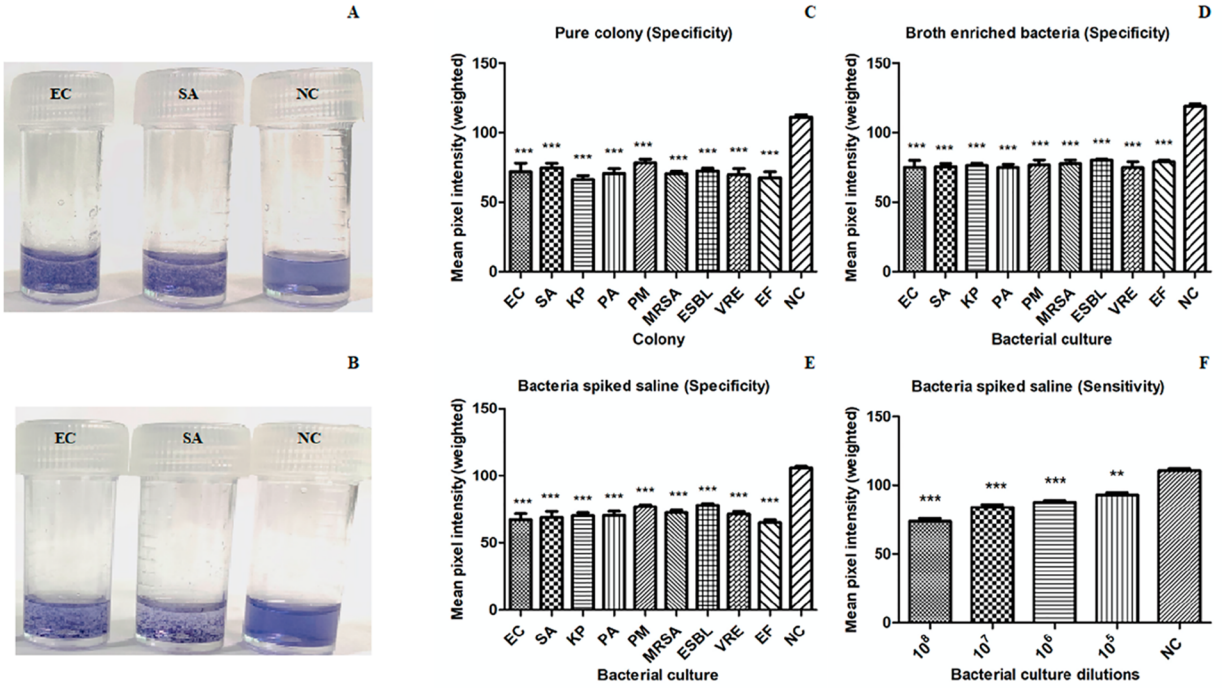

Figure 4. (A) Visible agglutination in EC and SA broth culture. (B) Agglutination observed in case of bacteria spiked saline suspension. Significant difference in intensity due to agglutination as observed in all the cultures compared to the negative control in case of (C) pure colony; (D) broth culture; (E) bacteria spiked saline suspension; (F) significant difference in intensity due to agglutination as observed in spiked saline with EC in graded concentrations as compared to negative control; p-value <0.01 (**), p-value <0.001 (***).

with dye entrapped lectin conjugated chitosan nanoparticles observed in CLSM (Figure 3A−C) and CRYO FEG-SEM (Figure 3D,E). Lectin from wheat germ agglutinin from *Triticum vulgaris* is known to bind to *N*-acetyl glucosamine, one of the monosaccharides that make up the pepetidoglycan cell wall of the bacterial cell. The chitosan nanoparticles when tagged with lectin have been observed to be able to detect both Gram-positive and Gram-negative cells and form visible agglutinants. Further, the dye entrapped chitosan nanoparticles help visualize the agglutinant.

***In Vitro* Analysis of Device.** The device showed agglutination in the presence of bacterial colony, broth culture, and bacteria-spiked saline suspensions at concentration of 10^8 cfu/mL (Figure 4A−E). The device, when checked for its limit of detection (LOD) in the case of saline dilutions, showed positive results in the form of agglutination up to 10^5 cfu/mL concentration as shown in (Figure 4F), while no visible agglutination was observed in the case of a 10^4 cfu/mL concentration of bacteria spiked in saline as compared to 10^5 cfu/mL and higher (Figure S1). On image analysis, a significant difference was observed between the mean weighted intensities of positive and negative samples which further confirm agglutination. As compared to the chitosan loaded nanoparticles, safranin loaded nanoparticles were found to give inaccurate results for different concentrations of bacteria (Figure S5).

To confirm its specificity for bacterial identification only, saline spiked fungal culture of CA two different concentrations was tested and found to have no visible agglutination confirmed by image analysis that showed nonsignificant difference as compared to negative control (Figure S2).

***In Vitro* Analysis of Device with Simulated Samples.** Furthermore, analysis of the device with ASM, using EC, SA, and KP exhibited agglutination and a significant difference at 10^8 cfu/mL as shown in Figure 5A,B. The LOD for ASM was observed to be 10^5 cfu/mL seen in Figure 5C. The visible agglutination and significant difference in the image analysis as compared to the negative control in all cases was indicative of specific detection of the presence of bacteria as compared to the absence of bacteria in a negative control sample. Further, the presence of bacteria was conformed for both Gram-positive as well as Gram-negative spiked bacterial samples indicative of the efficient detection of both by the developed device.

Similarly, respiratory and wound swabs showed positive results at 10^8 cfu/mL in the presence of respective bacteria spiked samples (Figure 5D,E,G,H), while the LOD values in both cases were found to be 10^5 cfu/mL (Figure 5F,I).

For evaluation of the urine mimicking medium, cultures both Gram-positive as well as Gram-negative bacteria were tested, exhibiting significant agglutination at 10^8 cfu/mL (Figure 5J,K). The LOD for each of the bacterial cultures spiked in simulated samples was found to be 10^5 cfu/mL as seen in Figure 5I for EC.

Confounding Factors. Each interfering agent was tested with 10^8 cfu/mL bacterial concentration of EC, and the device continued to exhibit positive results through visible agglutination. Similarly, samples devoid of culture showed no agglutination even in the presence of the interfering agents. This study confirmed that the developed device was suitable for clinical samples, as there was no interference that would confound the results through false positive or false negative readouts. Details of the pixel intensity of each of the above confounding factors are represented in Figure 6.

Stability and Reproducibility Analysis. Different batches of the device showed reproducible results with bacteria-spiked samples. No visual difference like discoloration or agglomeration was observed in the prepared nanomaterial when stored under accelerated conditions for 90 days.

https://doi.org/10.1021/acs.bioconjchem.2c00299
Bioconjugate Chem. 2022, 33, 1552−1563

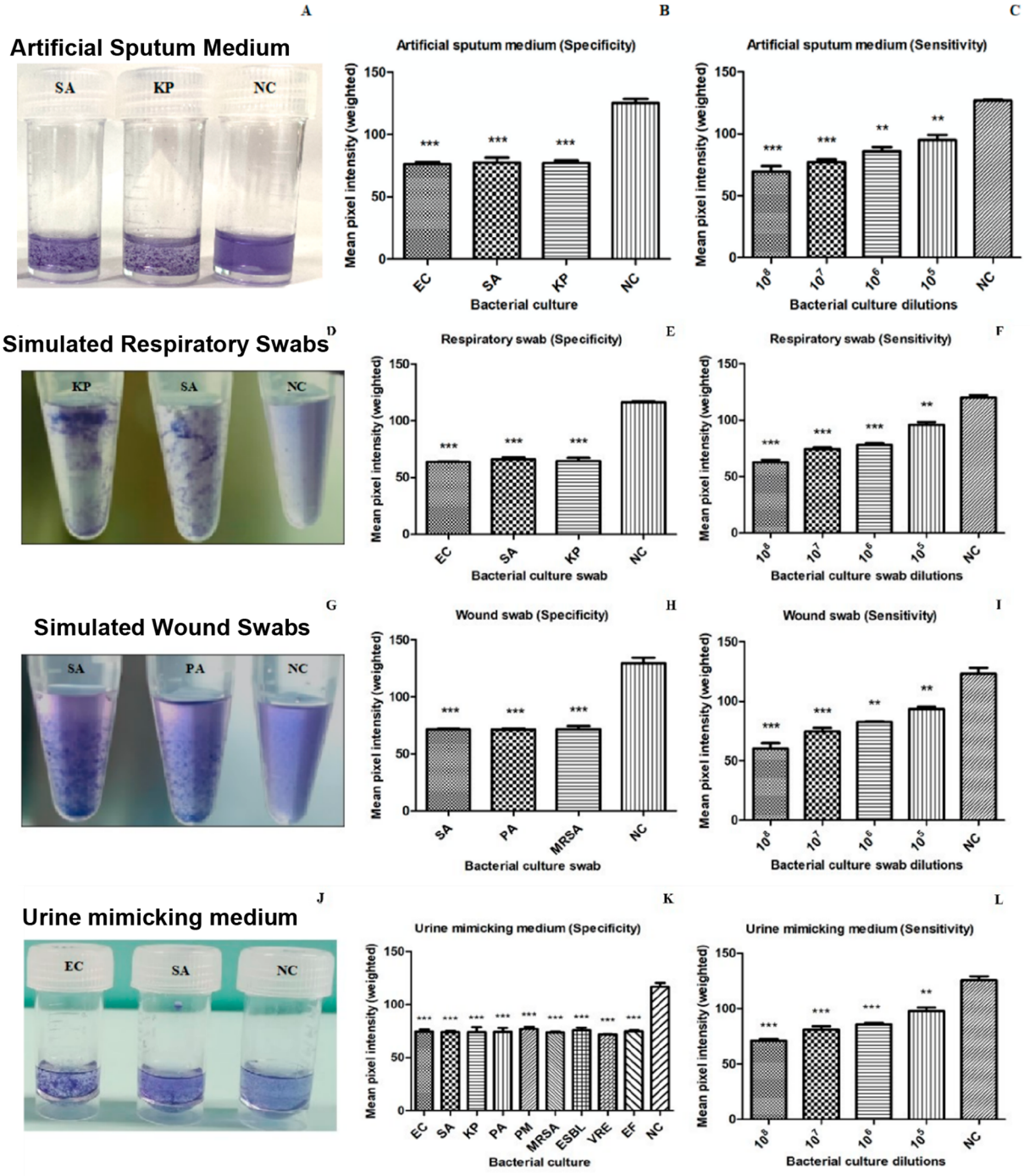

Figure 5. (A) Visible agglutination in SA and KP from spiked artificial sputum medium. (B) Significant difference in intensity due to agglutination for ASM samples of EC, SA, and KP as compared to the negative control (NC). (C) Significant difference in intensity due to agglutination in ASM sample of KP in graded concentrations as compared to negative control. (D) Visible agglutination in SA and KP in simulated respiratory swabs. (E) Significant difference in intensity due to agglutination for EC, SA, and KP as compared to the negative control in simulated and spiked respiratory swabs. (F) Significant difference for KP spiked in graded concentrations in simulated respiratory swabs. (G) Visible agglutination in cases of SA and PA spiked simulated wound swabs. (H) Significant difference in intensity due to agglutination for SA, PA, and MRSA, as compared to the negative control in the respiratory swab cultures. (I) Significant difference in intensity due to agglutination of SA spiked in graded concentrations. (J) Visible agglutination in EC and SA in urine mimicking medium. (K) Significant difference in intensity due to agglutination for all the bacteria spiked simulated urine samples as compared to negative control. (L) Significant difference in intensity due to agglutination in graded concentrations of EC as compared to negative control; p-value <0.01 (**), p-value <0.001 (***).

Subsequent analysis with samples containing bacteria corroborated in establishing the particles as a stable entity. These *in vitro* evaluations for reproducibility and stability were carried out using 10^8 cfu/mL bacterial concentration of EC (Figure 7). No significant difference was observed among various batches and at various time points confirming the reproducibility and stability of the device, respectively.

https://doi.org/10.1021/acs.bioconjchem.2c00299
Bioconjugate Chem. 2022, 33, 1552−1563

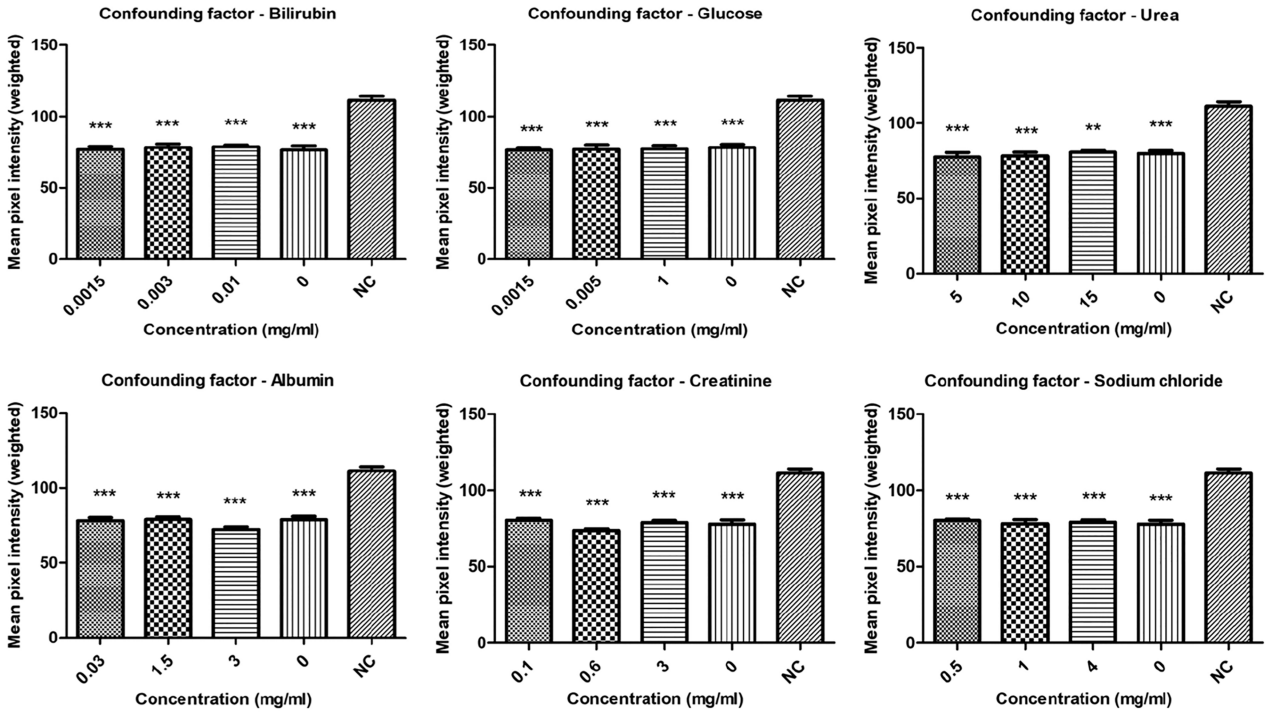

Figure 6. Significant difference in agglutination for various concentrations of different interfering factors assessed in the presence of EC as compared to the negative control (NC); *p*-value <0.01 (**), *p*-value <0.001 (***).

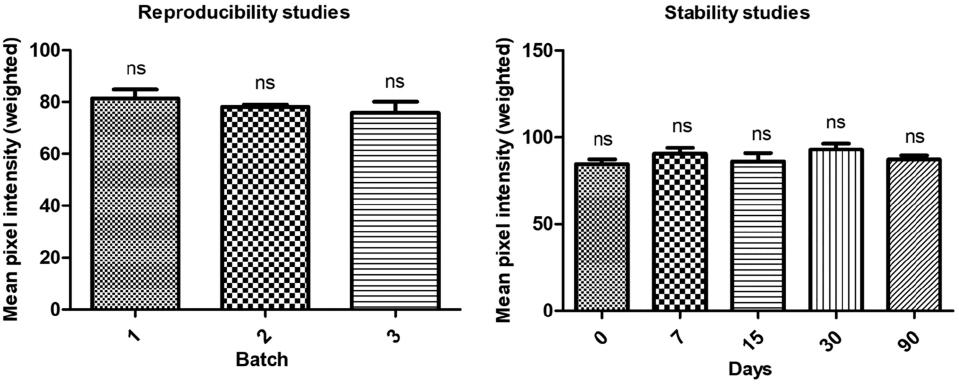

Figure 7. (left) Reproducibility of the device evaluated with three different batches of nanomaterial synthesized. (right) Accelerated stability of the device at regular time intervals. ns − not significant.

The Developed Device. The device has two components (Figure 8):

Primary vial (Vial 1): Sterile screw cap polypropylene vial that is optically clear, flat bottom, self-standing, airtight, and graduated (total volume: 5 mL) with transparent base. The primary vial contains 100 μL of the dye entrapped lectin conjugated chitosan nanoparticle suspension. This forms the basic unit of device in which the test is performed.

Secondary Vial (Vial 2): Sterile screw cap polypropylene vials (total volume: 1 mL) were used as secondary vials containing 1 M NaOH solution.

The developed device was packaged in convenient polypropylene vials containing nanomaterial in one and reagent (NaOH) in another along with a Pasteur pipet to add sample, all provided in hardbound packing material as seen in the Figure 8.

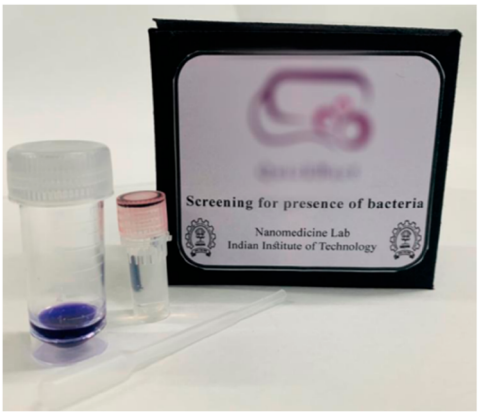

Figure 8. Developed point-of-care device.

https://doi.org/10.1021/acs.bioconjchem.2c00299
Bioconjugate Chem. 2022, 33, 1552−1563

DISCUSSION

Chitosan nanoparticles with entrapped substances have been reported to have varied sizes, which depend upon the ratio of chitosan to TPP, the size of the molecule entrapped, and the temperature of synthesis of particles. Study by Fan et al. states that an increase in chitosan to TPP ratio leads to greater particle size, while an increase in temperature leads to smaller particle size.[14] The hydrodynamic diameter of synthesized nanoparticles was found to be approximately 174 nm as obtained through DLS, and it lies in the range of 130−200 nm. The zeta potential of dye entrapped nanoparticles was 18.5 ± 0.9 mV. The zeta potential of the dye entrapped lectin conjugated chitosan nanoparticles increased to 26.2 ± 1.4 mV. The increase in zeta potential of nanoparticles due to conjugation of lectin from *Triticum vulgaris* (WGA) may be explained by the fact that WGA is positively charged, while most other lectins are negatively charged. Yin et al. recorded a similar increase in the zeta potential of PLGA nanoparticles upon conjugation with WGA.[15]

On addition of bacteria, visible agglutination was observed, which was confirmed using CLSM for both Gram-positive as well as Gram-negative bacteria. These results were corroborated by the SEM results, where nanoparticles were seen aggregating around micron-sized bacteria. The aggregation of the nanoparticles around bacterial cells led to visible agglutination in the nanoparticle suspension which was interpreted as a positive readout.

Lectins are pattern recognition proteins known for their specificity toward certain carbohydrates due to the presence of Carbohydrate Recognition Domains (CRD). Lectin from species *Triticum vulgaris* or wheat germ agglutinin (WGA) is known to be specific toward *N*-acetyl glucosamine (NAG) through binding with Ser62, Tyr64, and His66 residues of the lectin.[13] NAG is a carbohydrate known to be found abundantly in a primary bacterial cell wall component—peptidoglycan. While 95% of bacterial cell wall in Gram-positive bacteria is constituted of peptidoglycan, it makes up only 5% of the Gram-negative bacterial cell wall. The Gram-negative cell wall has an additional lipopolysaccharides (LPS) membrane with antigens immobilized on its outer surface. Thus, the basis of detection of Gram-negative bacteria could be attributed to the composition of the outer membrane. The various surface antigens contain NAG in them, and certain Gram-negative bacteria are known to have a polymer made up of NAG at the cell surface.[16] While the single interaction between the protein and the carbohydrate is relatively weaker than that of an antigen−antibody interaction, lectin-based interactions are known to be multivalent. This makes lectins effective recognition moieties which has relevance in agglutination-based tests that form the basis of the present device.

Previously, lectins have been used to detect certain species of bacteria such as *Staphylococcus aureus*, *Escherichia coli*, and *Bacillus subtilis*. Gasparyan et al. detailed a technique that utilizes anisotropic silver nanoparticles conjugated to potato lectin known to be specific for NAG and, additionally, can detect oligomers of N-acetylmuramic acid (NAM) for detection of *S. aureus*. However, the test could not be used for point-of-care detection of bacteria due to the requirements of long incubation time (3−4 h) and additional instrumentation for measuring optical spectra and due to the low stability of potato lectin over only a week.[16] The current study fits a point-of-care setting as it is capable of instrument-free detection of a variety of bacterial species through visible agglutination with bacteria at a low concentration of 10^5 cfu/mL. The nanoparticles used in this device were found to be stable for 3 months.

Another study by Yang et al. exploits the size tunability and surface plasmon resonance (SPR) properties of gold nanoparticles to detect *S. aureus* in blood using WGA and magnetic nanoparticles. The whole procedure involves multiple incubation steps and a turnaround time of 7 h. While its LOD is 3.5 cfu/mL, the technology finds no use in a point-of-care setting due to high dependence on surface plasmon resonance instrumentation and skilled personnel.[17]

In the present study, the *in vitro* analysis shows 100% specificity in colony and saline suspensions as well as broth culture samples. Subsequent analysis using the bacteria-spiked simulated samples also exhibited positive results in the presence of bacteria, further confirming 100% specificity in *in vitro* evaluations. In the case of urinary tract infections (UTI) significant bacteriuria occurs at 10^5 cfu/mL bacterial concentration and above.[18,19] This was considered as a cutoff concentration for analysis purposes. The *in vitro* analysis shows 100% sensitivity up to a concentration as low as 10^5 cfu/mL. The evaluation of device using interfering agents suggests that this device can be used in a clinical setup without leading to any confounding results. The nanomaterial used for developing such devices can be repurposed in smart wound dressings as described by Guo et al. to make a theranostic approach for detection as well as treatment of wound infections by the antimicrobial properties of chitosan and a completely biodegradable material.[20]

The most notable drawbacks of traditional microbiological cultivation techniques and rapid molecular techniques like polymerase chain reaction (PCR), next-generation sequencing, and surface−enhanced Raman spectroscopy (SERS) include additional steps like sequencing for PCR, use of sophisticated instruments, requirement of trained personnel, and the need of an isolated colony.[2,21,22] As compared to these techniques, the present technology can be categorized into a point-of-care device, as it fulfills the benchmark criteria of "ASSURED" as stated by the WHO.[9] The developed POCD shows promising results and, thus, can be used in remote areas with limited accessibility to avoid delayed treatment while ensuring rapid detection of bacterial infections. The device can be established as a mandatory screening tool for infections with nonspecific symptoms caused by a broad spectrum of pathogens.

CONCLUSION

Based on the *in vitro* analysis, the developed device facilitated the point-of-care detection of bacterial against nonbacterial infections within 10 min in a wide variety of samples with 100% sensitivity and specificity. The results can be detected visually and are easy to interpret. This device fulfills criteria of being affordable, easy to use, and rapid and, hence, qualifies as a point-of-care device to screen clinical samples for the presence of bacteria.

EXPERIMENTAL SECTION

Materials. Chitosan (85−90% deacetylated) was purchased from Marine Chemicals, India. Sodium tripolyphosphate (TPP) (97−99% purity), 2-(*N*-morpholino)ethanesulfonic acid (MES) buffer, *N*-(3-(dimethylamino)propyl)-*N*′-ethyl-carbodiimide hydrochloride (EDC), *N*-hydroxysuccinimide

https://doi.org/10.1021/acs.bioconjchem.2c00299
Bioconjugate Chem. 2022, 33, 1552−1563

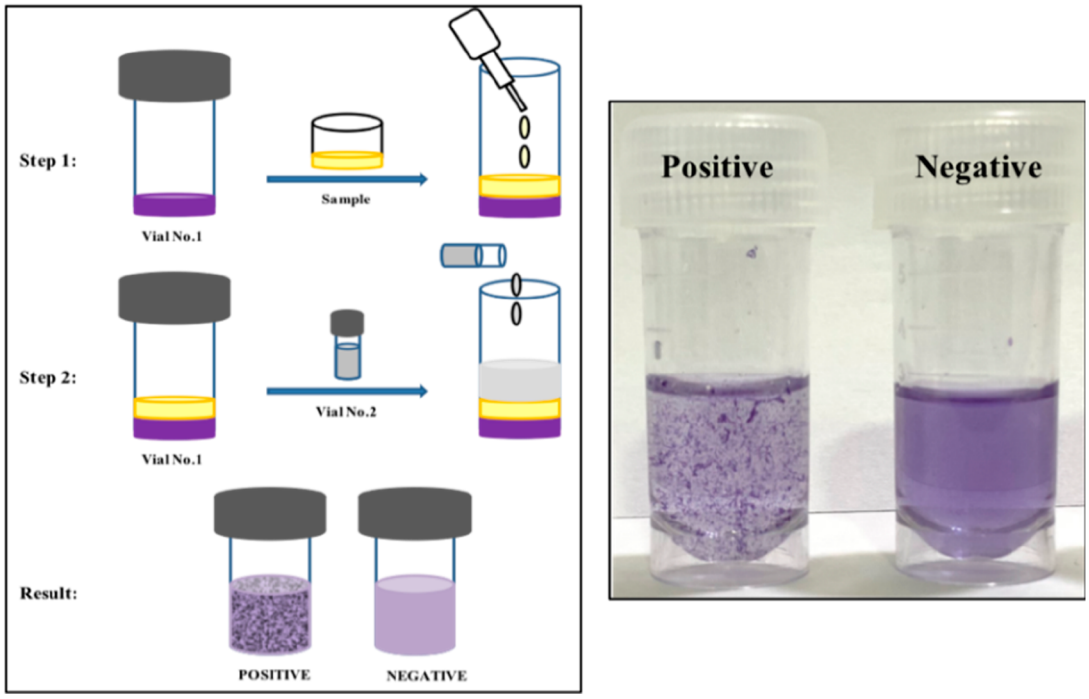

Figure 9. Schematic of test protocol (left); Actual images of visual readouts (right).

(NHS), phosphotungstic acid (PTA), sodium hydroxide (NaOH), crystal violet, and safranin were obtained from Himedia Laboratories, LLC, India. Dialysis membrane-50 (molecular weight cutoff: 12−14 kDa) and 0.5 McFarland Standard were also obtained from Himedia Laboratories, LLC, India. Glacial acetic acid (100% pure) was obtained from Merck, India. *Triticum vulgaris* Wheat Germ Agglutinin (WGA) was obtained from Sigma-Aldrich, USA.

Bacterial Cultures. Bacterial species were cultured, namely, *Escherichia coli* ATCC 25922 (EC), *Staphylococcus aureus* ATCC 25923 (*mecA* negative) (SA), *Klebsiella pneumoniae* ATCC 10031 (KP), *Pseudomonas aeruginosa* ATCC 27853 (PA), *Proteus mirabilis* ATCC 21100 (PM), *Staphylococcus aureus* ATCC 43300 (*mecA* positive) (MRSA), *Klebsiella pneumoniae* ATCC 700603 (ESBL), *Enterococcus faecalis* ATCC 29212 (EF), and *Enterococcus faecalis* ATCC 51299 (VRE).

Fungal culture. *Candida albicans* ATCC 10231 (CA). Pure colony isolates were used to prepare culture suspensions in sterile 0.9% saline. Turbidity was matched with 0.5 McFarland Standard to obtain 1×10^8 cfu/mL and serially diluted up to 1×10^4 cfu/mL. In the case of broth cultures, a pure isolated colony was inoculated in sterile Nutrient Broth and incubated at 37 °C for 16−18 h.

Synthesis of Crystal Violet-Entrapped Lectin-Functionalized Chitosan Nanoparticles. Chitosan nanoparticles were prepared by suitable modifications to the ionic gelation method to achieve dye entrapped nanoparticles.[23] Acetic acid (1%) was used to prepare 3 mM crystal violet solution. After heating the dye solution to 70 °C, chitosan (85−90% deacetylation) was dissolved at a concentration of 1 mg/mL under constant stirring. Tripolyphosphate solution at a concentration of 0.005% was added to the chitosan solution to synthesize dye entrapped chitosan nanoparticles. Biomolecular conjugation of lectin with dye entrapped chitosan nanoparticles was achieved by adding 0.2% (w/v) each of EDC and 0.2% (w/v) NHS in 1:1 molar ratio to 1 mg lectin from *Triticum vulgaris* Wheat Germ Agglutinin (WGA) in 0.05 M MES. Nanoparticles without conjugation were used for assessing the sensitivity and specificity of the device due to incorporation of lectin (Figures S6 and S7).

Subsequently, placed in a dialysis membrane and dialyzed against a solution of 0.05 M MES buffer for 2 h under stirring. Chitosan nanoparticle suspension was centrifuged at 10,000*g* for 20 min at 16 °C. The supernatant was discarded, and nanoparticles were resuspended in 7 mL of 0.05 M MES buffer and sonicated. To this, the EDC-NHS conjugated lectin suspension within the dialysis membrane was added, and the mixture was vortexed for 1 h at room temperature to allow biomolecular conjugation. The suspension was stored at 4 °C until further use. Additionally, safranin loaded chitosan nanoparticles were also synthesized to determine the validity of nanomaterial for different dyes (Figure S4).

Characterization of Nanoparticles. Chitosan nanoparticles were analyzed for morphology using CRYO-FEG-SEM (JSM-7600F, field emission gun scanning electron microscope, JEOL Ltd., Japan), with Cryo Unit (PP3000T) Quorum Technologies, UK, SEI resolution: 1.5 nm (1 kV) in GB mode; 1.0 nm (15 kV)) and FEG-TEM (field emission gun transmission electron microscope JEM-2100F, JEOL Ltd., Japan, accelerating voltage: 200 kV, resolution: point, 0.19 nm; line, 0.1 nm) by preparing suitable dilutions of the nanoparticle suspension and mixing with 10 μL of 2% phosphotungstic acid (PTA) for imaging purposes. The nanoparticle suspension was analyzed for its hydrodynamic diameter and zeta potential using Nano ZS90 Zetasizer, (Malvern Panalytical Ltd., UK). Both conjugated and nonconjugated nanoparticles were characterized to confirm the difference in the nanomaterial and its relative potential to detection of bacteria in a sample.

Test Protocol. The procedure for detection of bacteria was an easy to perform two-step process. The first step required addition of 100 μL sample in the primary vial. This was

https://doi.org/10.1021/acs.bioconjchem.2c00299
Bioconjugate Chem. 2022, 33, 1552−1563

followed by addition of 200 μL of 1 M NaOH from the secondary vial. A positive result denoting the presence of bacteria was confirmed by visible agglutination in the vial, whereas the absence of bacteria was indicated by a single-phase violet-colored suspension (Figure 9). Cut-off TOD for visible agglutination-based results was 10 min.

Proof-of-Concept. Agglutination and binding of lectin conjugated chitosan nanoparticles to the surface of bacteria was confirmed by SEM and confocal laser scanning microscopy (CLSM) (Olympus (IX 81), Tokyo, Japan) and Fluoview 500. For this process, crystal violet was replaced with a cationic dye like safranin having excitation wavelength at 452 nm and emission wavelength at 544 nm for fluorescence spectrophotometric results, to avoid the additional use of staining and contrast agents (Figure S3a−c). The agglutinates in a positive reaction were separated and resuspended in phosphate buffer saline (PBS), placed on clear grease-free slides covered by coverslips. The coverslip was sealed using a sealing paint to avoid displacement and drying and then the prepared sample was subject to confocal analysis.

***In Vitro* Analysis.** For *in vitro* analysis of the device, bacteria and fungi spiked saline suspensions were prepared as mentioned in Microscopic Confirmation of Agglutination. The spiked saline suspensions were subjected to device in volume 100 μL followed by addition of NaOH reagent as per the testing protocol described in Confounding Factors. Similarly, bacterial cultures grown in broth and incubated overnight were also subjected to devices and test protocol followed as above. To further validate the device. simulated urine, sputum, respiratory swabs, and wound swabs were used including eukaryotic cells in such samples.

***In Vitro* Analysis Using Simulated Samples.** For this, fibroblast eukaryotic cell lines from mouse C3H (L929) ATCC CCL-1 and primary human foreskin fibroblast (HFF-1) ATCC SCRC-1041 acquired from Thermo Fisher Scientific were maintained in sterile Dulbecco's Modified Eagle Medium (DMEM) supplemented with 10% fetal bovine serum (FBS) and 1% antibiotic−antimycotic solution, incubated at 37 °C with 5% CO_2 in T-25 flasks. Upon 80% confluency, cells were trypsinized and neutralized by subjecting them to complete medium with 10% FBS and centrifuged. The pellet was washed and resuspended in sterile PBS. The cells were counted using a hemocytometer under a 10× lens following the Trypan blue cell viability count method. These cells were essentially used to mimic the simulated sample in the case of respective infections.[24] The following artificial samples were prepared and spiked with eukaryotic and bacterial cultures to be used as samples for testing.

Artificial Sputum Medium (ASM). This is a simulated medium which contains the components of respiratory secretion, including mucin, amino acids, free DNA, and others. Its composition mimics the sputum sample and was prepared according to the protocol developed by Dinesh et al. and Kirchner et al.[25,26] ASM was observed to be a pale, slightly turbid but free-flowing liquid medium that is chemically and biochemically similar to an actual sputum. Addition of 0.75% carrageenan sodium salts in ASM results in forming simulated sputum of a viscoelastic nature as original sputum; evaluation of the viscosity was carried out by performing rheology and found to be similar to that of upper respiratory infected sputum samples.[27] Saline suspensions of EC, SA, and KP and that of L929 cells were spiked with simulated sputum samples such that the viscosity was maintained and the final concentrations of bacteria were in the range of 10^5−10^8 cfu/mL, while that of L929 was 10^6 cells/mL.[28−30] The spiked simulated samples were then subjected to testing using the devices by adding 100 μL of the prepared sample and observing for agglutination. The positive samples showed agglutination due to the presence of bacteria, while those without both cell types (i.e., simulated sputum only) and with only L929 cells (i.e., without bacteria) remained as a violet-colored suspension without any visible agglutination.

Respiratory Swab. The ASM was used for the preparation of an artificial respiratory swab. This was spiked using bacterial cultures of EC, SA, or KP individually at counts of 10^5−10^8 cfu/mL along with L929 cells in a concentration of 10^6 cells/mL.[29,31] A sterile cotton swab was soaked in the prepared artificial medium spiked with bacterial and eukaryotic cells and used for testing. The simulated respiratory swab was subjected to a diluent (sterile PBS) for 5 min, rotated well to retrieve bacterial cells. 100 μL of this diluent was further used as a sample for analysis for testing the device as per the protocol described above.

Wound Swab. In the case of wound infections, fluid from the wound is collected on a swab.[32] This wound fluid is also referred to as wound exudate. Therefore, to simulate a wound swab, simulated wound exudate was prepared. FBS with sterile Maximum Recovery Diluent (comprising peptone and other salts) were mixed in 1:1 ratio, to prepare the Simulated Wound Exudate (SWE).[33] This was spiked with varied concentrations of SA, PA, or MRSA[34] along with the HFF cells.[35] The saline suspensions of bacterial cells and HFF cells were spiked in SWE such that bacterial concentation of 10^5−10^8 cfu/mL along with HFF cells 10^6 cells/mL was achieved in the simulated wound sample. A sterile cotton swab was soaked in the spiked simulated wound exudate and used for further analysis as mentioned for respiratory swab samples.

Urine Mimicking Medium. A simple medium mimicking normal human urine was prepared in PBS consisting of various organic and inorganic components like urea (170 mM), creatinine (7 mM), sodium chloride (90 mM), disodium phosphate (7 mM), and dipotassium hydrogen phosphate (7 mM).[36] The entire panel of bacterial cultures mentioned in Microscopic Confirmation of Agglutination was used for the analysis using urine mimicking medium with varying concentrations of bacterial cells and fixed concentration of eukaryotic cells present in normal human urine.[37−39]

Sensitivity and Specificity of the Device. To determine the specificity of the device, various bacteria at concentrations of 10^8 cfu/mL were screened. Similarly, to determine the limit of detection (LOD) and sensitivity, a graded concentration of bacteria ranging 10^8−10^4 cfu/mL were tested for all simulated samples. The range of bacterial concentration was selected based on the type of samples to be evaluated. In the case of urinary tract infections typical bacteriuria is confirmed for bacterial concentration of 10^5 cfu/mL,[40] while in the case of respiratory infections a sputum sample with bacterial concentration of $>10^7$ cfu/mL was considered for significant infection.[41]

Confounding Factors. The device is projected to be used for various types of clinical samples like urine, sputum, respiratory swabs, and wound swabs to determine the presence of bacteria in the case of an infection. Certain components in these samples may act as interfering factors and lead to variability in results. To ensure consistency in test results, the crystal violet entrapped lectin conjugated chitosan nano-

https://doi.org/10.1021/acs.bioconjchem.2c00299
Bioconjugate Chem. 2022, 33, 1552−1563

particles were assessed using six commonly occurring endogenous interfering factors in urine and other samples for causing any interference in the visible readout due to their presence. A wide range of concentrations of these compounds were added along with bacterial suspensions to simulate such extreme conditions and evaluate the devices. The factors and their range of concentrations in mg/mL for each were bilirubin (0.001−0.01),[42] glucose (0.0015−1),[43,44] urea (5−15),[45] albumin (0.03−0.3),[46−48] creatinine (0.1−3),[49] and sodium chloride (0.5−4).[50]

Stability and Reproducibility Studies. Since the nanoparticles were present in suspension in the final device, accelerated testing was performed using the International Council for Harmonization (ICH) guidelines for stability of the device.[51,52] The devices were vacuum sealed and tested under accelerated conditions of stability. For this, the devices were stored in a humidity chamber (Newtronic Lifecare Equipment Pvt. Ltd., India) adjusted at 40 °C and 75% relative humidity and evaluated with bacterial saline suspensions at 0, 7, 15, 30, and 90 days of storage. To ensure the reproducibility, at least three different batches of the dye entrapped lectin conjugated chitosan nanoparticles were evaluated with bacteria spiked saline suspensions.

Image Analysis. Images of the vials were obtained using iPhone XR (Generation 10 iOS) in the high dynamic range (HDR) mode. The photographed images were further analyzed through ImageJ (v 2.0.0-rc-69/1.52p, NIH, USA). For the analysis of agglutination in samples, weighted intensity was measured through the histogram function in ImageJ. This was performed within a region of interest (ROI) in the area of the image showing visible agglutination in the vial. Every sample was analyzed in triplicate with suitable negative controls (NC). Higher intensity indicated higher weighted sum of the red, green, and blue channels within the ROI, which is representative of the white color. The weighted intensities of the positive samples showing agglutination was expected to be significantly different from those for the negative samples showing no agglutination.

Statistical Analysis. The data obtained was represented as mean ± standard deviation. All statistical analysis was performed in Graph Pad Prism (v 5.01). A p-value of less than 5% was considered significant. The level of significance was determined through Student's t test and Analysis of Variance (ANOVA) followed by suitable post-tests. All experiments were performed in triplicate (n = 3).

■ ASSOCIATED CONTENT

Supporting Information

The Supporting Information is available free of charge at https://pubs.acs.org/doi/10.1021/acs.bioconjchem.2c00299.

Figures illustrating limit of detection, visible agglutination, imaging and methods (PDF)

■ AUTHOR INFORMATION

Corresponding Author

Kapil Punjabi − *Nanomedicine Lab, Department of Bioscience & Bioengineering, Indian Institute of Technology-Bombay, Mumbai 400 076, India;* orcid.org/0000-0002-1610-7633; Email: kapil9372@gmail.com

Authors

Rishi Rajat Adhikary − *Nanomedicine Lab, Department of Bioscience & Bioengineering, Indian Institute of Technology-Bombay, Mumbai 400 076, India*

Aishani Patnaik − *Nanomedicine Lab, Department of Bioscience & Bioengineering, Indian Institute of Technology-Bombay, Mumbai 400 076, India*

Prachi Bendale − *Nanomedicine Lab, Department of Bioscience & Bioengineering, Indian Institute of Technology-Bombay, Mumbai 400 076, India*

Survanshu Saxena − *Nanomedicine Lab, Department of Bioscience & Bioengineering, Indian Institute of Technology-Bombay, Mumbai 400 076, India*

Rinti Banerjee − *Nanomedicine Lab, Department of Bioscience & Bioengineering, Indian Institute of Technology-Bombay, Mumbai 400 076, India;* orcid.org/0000-0002-6400-5906

Complete contact information is available at: https://pubs.acs.org/10.1021/acs.bioconjchem.2c00299

Notes

The authors declare no competing financial interest.

■ ACKNOWLEDGMENTS

The authors are thankful to IMPRINT India for funding the project, Sophisticated Analytical Instrument Facility (SAIF) and Industrial Research and Consultancy Centre (IRCC) at the Indian Institute of Technology Bombay (IITB) for characterization studies. We dedicate this work to Late Prof. Rinti Banerjee, who passed away last year. This work would have not been possible without her guidance and support. We will miss her and be indebted to her for enlightening us with her immense knowledge and humility.

■ REFERENCES

(1) World Health Organization. *Global Health Estimates: Leading Causes of Death*; Geneva, 2018.

(2) Livermore, D. M.; Wain, J. Revolutionising Bacteriology to Improve Treatment Outcomes and Antibiotic Stewardship. *Infection & Chemotherapy* **2013**, *45* (1), 1.

(3) Kozel, T. R.; Burnham-Marusich, A. R. Point-of-Care Testing for Infectious Diseases: Past, Present, and Future. *J. Clin. Microbiol.* **2017**, *55* (8), 2313−2320.

(4) Peeling, R. W.; Mabey, D. Point-of-Care Tests for Diagnosing Infections in the Developing World. *Clinical Microbiology and Infection* **2010**, *16* (8), 1062−1069.

(5) Ahmed, A.; Rushworth, J. v.; Hirst, N. A.; Millner, P. A. Biosensors for Whole-Cell Bacterial Detection. *Clin. Microbiol. Rev.* **2014**, *27* (3), 631−646.

(6) Procop, G. W. *Koneman's Color Atlas and Textbook of Diagnostic Microbiology*; 2017.

(7) Tsalik, E. L.; Bonomo, R. A.; Fowler, V. G. New Molecular Diagnostic Approaches to Bacterial Infections and Antibacterial Resistance. *Annual Review of Medicine* **2018**, *69* (1), 379−394.

(8) Langley, G.; Besser, J.; Iwamoto, M.; Lessa, F. C.; Cronquist, A.; Skoff, T. H.; Chaves, S.; Boxrud, D.; Pinner, R. W.; Harrison, L. H. Effect of Culture-Independent Diagnostic Tests on Future Emerging Infections Program Surveillance. *Emerg Infect Dis* **2015**, *21* (9), 1582−1588.

(9) Kosack, C. S.; Page, A.-L.; Klatser, P. R. A Guide to Aid the Selection of Diagnostic Tests. *Bull. World Health Organ* **2017**, *95* (9), 639−645.

(10) Verma, R.; Adhikary, R. R.; Banerjee, R. Smart Material Platforms for Miniaturized Devices: Implications in Disease Models and Diagnostics. *Lab Chip* **2016**, *16* (11), 1978−1992.

(11) Punjabi, K.; Adhikary, R. R.; Patnaik, A.; Bendale, P.; Singh, S.; Saxena, S.; Banerjee, R. Core−Shell Nanoparticles as Platform Technologies for Paper Based Point-of-Care Devices to Detect Antimicrobial Resistance. *J. Mater. Chem. B* **2020**, *8* (29), 6296−6306.
(12) Bugnicourt, L.; Ladavière, C. Interests of Chitosan Nanoparticles Ionically Cross-Linked with Tripolyphosphate for Biomedical Applications. *Prog. Polym. Sci.* **2016**, *60*, 1−17.
(13) Muraki, M.; Ishimura, M.; Harata, K. Interactions of Wheat-Germ Agglutinin with GlcNAcβ1,6Gal Sequence. *Biochimica et Biophysica Acta (BBA) - General Subjects* **2002**, *1569* (1−3), 10−20.
(14) Fan, W.; Yan, W.; Xu, Z.; Ni, H. Formation Mechanism of Monodisperse, Low Molecular Weight Chitosan Nanoparticles by Ionic Gelation Technique. *Colloids Surf., B* **2012**, *90*, 21−27.
(15) Yin, Y.; Chen, D.; Qiao, M.; Lu, Z.; Hu, H. Preparation and Evaluation of Lectin-Conjugated PLGA Nanoparticles for Oral Delivery of Thymopentin. *J. Controlled Release* **2006**, *116* (3), 337−345.
(16) Konopka, J. B. N-Acetylglucosamine Functions in Cell Signaling. *Scientifica (Cairo)* **2012**, *2012*, 1−15.
(17) Yang, G.; Meng, X.; Wang, Y.; Yan, M.; Aguilar, Z. P.; Xu, H. 2-Step Lectin-Magnetic Separation (LMS) Strategy Combined with AuNPs-Based Colorimetric System for S. Aureus Detection in Blood. *Sens. Actuators, B* **2019**, *279*, 87−94.
(18) Coulthard, M. G.; Kalra, M.; Lambert, H. J.; Nelson, A.; Smith, T.; Perry, J. D. Redefining Urinary Tract Infections by Bacterial Colony Counts. *Pediatrics* **2010**, *125* (2), 335−341.
(19) Kwon, J. H.; Fausone, M. K.; Du, H.; Robicsek, A.; Peterson, L. R. Impact of Laboratory-Reported Urine Culture Colony Counts on the Diagnosis and Treatment of Urinary Tract Infection for Hospitalized Patients. *American Journal of Clinical Pathology* **2012**, *137* (5), 778−784.
(20) Dong, R.; Guo, B. Smart Wound Dressings for Wound Healing. *Nano Today* **2021**, *41*, 101290.
(21) Budding, A. E.; Hoogewerf, M.; Vandenbroucke-Grauls, C. M. J. E.; Savelkoul, P. H. M. Automated Broad-Range Molecular Detection of Bacteria in Clinical Samples. *J. Clin. Microbiol.* **2016**, *54* (4), 934−943.
(22) Pearson, B.; Mills, A.; Tucker, M.; Gao, S.; McLandsborough, L.; He, L. Rationalizing and Advancing the 3-MPBA SERS Sandwich Assay for Rapid Detection of Bacteria in Environmental and Food Matrices. *Food Microbiology* **2018**, *72*, 89−97.
(23) Calvo, P.; Remuñan-López, C.; Vila-Jato, J. L.; Alonso, M. J. Chitosan and Chitosan/Ethylene Oxide-Propylene Oxide Block Copolymer Nanoparticles as Novel Carriers for Proteins and Vaccines. *Pharm. Res.* **1997**, *14* (10), 1431−1436.
(24) Freshney, R. I. *Culture of Animal Cells*; John Wiley & Sons, Inc.: Hoboken, NJ, USA, 2010. DOI: 10.1002/9780470649367.
(25) Diraviam Dinesh, S.; Diraviam Dinesh, S. Artificial Sputum Medium. *Protocol Exchange* **2010**, DOI: 10.1038/protex.2010.212.
(26) Kirchner, S.; Fothergill, J. L.; Wright, E. A.; James, C. E.; Mowat, E.; Winstanley, C. Use of Artificial Sputum Medium to Test Antibiotic Efficacy Against <Em>Pseudomonas Aeruginosa</Em> in Conditions More Relevant to the Cystic Fibrosis Lung. *J. Visualized Exp.* **2012**, No. 64, 1 DOI: 10.3791/3857.
(27) Hirose, R.; Nakaya, T.; Naito, Y.; Daidoji, T.; Watanabe, Y.; Yasuda, H.; Konishi, H.; Itoh, Y. Viscosity Is an Important Factor of Resistance to Alcohol-Based Disinfectants by Pathogens Present in Mucus. *Sci. Rep.* **2017**, *7* (1), 13186.
(28) Cukic, V.; Hadzic, A. The Most Common Detected Bacteria in Sputum of Patients with Community Acquired Pneumonia (CAP) Treated In Hospital. *Medical Archives* **2016**, *70* (5), 354.
(29) Jonas, M. Bacteremic Escherichia Coli Pneumonia. *Archives of Internal Medicine* **1982**, *142* (12), 2157.
(30) Popov, T.; Gottschalk, R.; Kolendowicz, R.; Dolovich, J.; Powers, P.; Hargreave, F. E. The Evaluation of a Cell Dispersion Method of Sputum Examination. *Clinical and Experimental Allergy* **1994**, *24* (8), 778−783, DOI: 10.1111/j.1365-2222.1994.tb00990.x.
(31) Dasaraju, P. V.; Liu, C. Infections of the Respiratory System. In *Medical Microbiology*, 4th ed.; University of Texas Medical Branch at Galveston: Galveston, TX,, 1996; Chapter 93.
(32) Smith, M. E.; Robinowitz, N.; Chaulk, P.; Johnson, K. Comparison of Chronic Wound Culture Techniques: Swab versus Curetted Tissue for Microbial Recovery. *Br J. Community Nurs* **2014**, *19*, S22−6.
(33) Said, J.; Dodoo, C. C.; Walker, M.; Parsons, D.; Stapleton, P.; Beezer, A. E.; Gaisford, S. An in Vitro Test of the Efficacy of Silver-Containing Wound Dressings against Staphylococcus Aureus and Pseudomonas Aeruginosa in Simulated Wound Fluid. *Int. J. Pharm.* **2014**, *462* (1−2), 123−128.
(34) Pondei, K.; Fente, B. G.; Oladapo, O. Current Microbial Isolates from Wound Swabs, Their Culture and Sensitivity Pattern at the Niger Delta University Teaching Hospital, Okolobiri, Nigeria. *Trop Med. Health* **2013**, *41* (2), 49−53.
(35) Trøstrup, H.; Lundquist, R.; Christensen, L. H.; Jorgensen, L. N.; Karlsmark, T.; Haab, B. B.; Agren, M. S. S100A8/A9 Deficiency in Nonhealing Venous Leg Ulcers Uncovered by Multiplexed Antibody Microarray Profiling. *Br J. Dermatol* **2011**, *165* (2), 292−301.
(36) Brooks, T.; Keevil, C. W. A Simple Artificial Urine for the Growth of Urinary Pathogens. *Lett. Appl. Microbiol* **1997**, *24* (3), 203−206.
(37) Behzadi, P.; Behzadi, E.; Yazdanbod, H.; Aghapour, R.; Akbari Cheshmeh, M.; Salehian Omran, D. A Survey on Urinary Tract Infections Associated with the Three Most Common Uropathogenic Bacteria. *Maedica* **2010**, *5* (2), 111−115.
(38) ROFE, P. The Cells of Normal Human Urine; a Quantitative and Qualitative Study Using a New Method of Preparation. *J. Clin Pathol* **1955**, *8* (1), 25−31.
(39) Silver, S. A.; Baillie, L.; Simor, A. E. Positive Urine Cultures: A Major Cause of Inappropriate Antimicrobial Use in Hospitals. *Canadian Journal of Infectious Diseases and Medical Microbiology* **2009**, *20* (4), 107−111.
(40) Wilson, M. L.; Gaido, L. Laboratory Diagnosis of Urinary Tract Infections in Adult Patients. *Clin Infect Dis* **2004**, *38* (8), 1150−1158.
(41) Baquero, F.; Alvarez, M.-E.; Cantón, R. Bacteriologic Diagnosis of Respiratory Tract Infections. *Clin Microbiol Infect* **1996**, *1*, S10−S15.
(42) VanWagner, L. B.; Green, R. M. Evaluating Elevated Bilirubin Levels in Asymptomatic Adults. *JAMA* **2015**, *313* (5), 516.
(43) Walker, H. K. *Clinical Methods: The History, Physical, and Laboratory Examinations*, 3rd ed.; Butterworths: Boston, 1990.
(44) Hieshima, K.; Sugiyama, S.; Yoshida, A.; Kurinami, N.; Suzuki, T.; Ijima, H.; Miyamoto, F.; Kajiwara, K.; Jinnouchi, K.; Jinnouchi, T.; Jinnouchi, H. Elevation of the Renal Threshold for Glucose Is Associated with Insulin Resistance and Higher Glycated Hemoglobin Levels. *Journal of Diabetes Investigation* **2020**, *11* (3), 617−625.
(45) Liu, L.; Mo, H.; Wei, S.; Raftery, D. Quantitative Analysis of Urea in Human Urine and Serum by ^{1}H Nuclear Magnetic Resonance. *Analyst* **2012**, *137* (3), 595−600.
(46) Coskun, A. F.; Nagi, R.; Sadeghi, K.; Phillips, S.; Ozcan, A. Albumin Testing in Urine Using a Smart-Phone. *Lab Chip* **2013**, *13* (21), 4231.
(47) Huang, Y.; Cao, Y.; Zou, M.; Luo, X.; Jiang, Y.; Xue, Y.; Gao, F. A Comparison of Tissue versus Swab Culturing of Infected Diabetic Foot Wounds. *International Journal of Endocrinology* **2016**, *2016*, 1−6.
(48) Shimura, S.; Sasaki, T.; Sasaki, H.; Takishima, T. Chemical Properties of Bronchorrhea Sputum in Bronchial Asthma. *Chest* **1988**, *94* (6), 1211−1215.
(49) Barr, D. B.; Wilder, L. C.; Caudill, S. P.; Gonzalez, A. J.; Needham, L. L.; Pirkle, J. L. Urinary Creatinine Concentrations in the U.S. Population: Implications for Urinary Biologic Monitoring Measurements. *Environ. Health Perspect.* **2005**, *113* (2), 192−200.
(50) Hato, T.; Ng, R. Diagnostic Value of Urine Sodium Concentration in Hyponatremia Due to Syndrome of Inappropriate Antidiuretic Hormone Secretion versus Hypovolemia. *Hawaii Med. J.* **2010**, *69* (11), 264−267.

(51) Abolhasani, A.; Biria, D.; Abolhasani, H.; Zarrabi, A.; Komeili, T. Investigation of the Role of Glucose Decorated Chitosan and PLGA Nanoparticles as Blocking Agents to Glucose Transporters of Tumor Cells. *Int. J. Nanomed.* **2019**, *14*, 9535−9546.
(52) Szymańska, E.; Winnicka, K. Stability of Chitosan—A Challenge for Pharmaceutical and Biomedical Applications. *Marine Drugs* **2015**, *13* (4), 1819−1846.

https://doi.org/10.1021/acs.bioconjchem.2c00299
Bioconjugate Chem. 2022, 33, 1552−1563